Chemistry

Physical & Theoretical Chemistry fields

Okayama University *Year* 1997

Shape evolution of electrodeposited bumps with deep cavity

Kazuo Kondo
Okayama University

Keisuke Fukui
Himeji Institute of Technology

n_i moles of species i
X_i cationic fraction of species i

REFERENCES

1. G. H. Kesall and R. A. Williams, *This Journal*, **138**, 931 (1991).
2. W. B. Crow, J. R. Myers, and J. V. Jeffreys, *Corrosion*, **28**, 77 (1972).
3. A. T. Kuhn, R. B. Lartey, D. W. Wakeman, and N. El-Nasr, *Br. Corros. J.*, **13**, 123 (1978).
4. Y. Omurtag and M. Doruk, *Corros. Sci.*, **10**, 225 (1970).
5. U. Wolff, Private communication.
6. S. Haupt, C. Calinski, U. Collisi, H. W. Hoppe, H. D. Speckmann, and H.-H. Strehblow, *Surf. Interface Anal.*, **9**, 357 (1986).
7. J. M. Sanz and S. Hofmann, *Surf. Interface Anal.*, **5**, 210 (1983).
8. D. A. Shirley, *Phys. Rev. B*, **5**, 4709 (1972).
9. D. Schaepers and H.-H. Strehblow, *This Journal*, **142**, 2210 (1995).
10. J. H. Scofield, *J. Electron Spectrosc.*, **8**, 129 (1976).
11. G. C. Nelson, *J. Vac. Sci. Technol. A*, **4**, 1567 (1986).

Current Evolution of Electrodeposited Copper Bumps with Photoresist Angle

Kazuo Kondo*

Faculty of Engineering, University of Okayama, Okayama 700, Japan

Keisuke Fukui

Himeji Institute of Technology, Himeji 671-22, Japan

ABSTRACT

We report the current distribution of copper bumps with photoresist sidewall angles. The role of outer diffusion, vortices, and penetration flow within the cavity is discussed, with numerical fluid dynamics computed in order to prevent side bumping. The current distributions were calculated at the diffusion controlled overpotential. The mass transfer-limited current distribution showed that a zero or negative angle reduced diffusion from the outer surroundings and enhanced vortex formation at the cathode corners. Reduction in the diffusion and enhancement in vortices reduced current at the cathode corners and prevented side bumping.

Introduction

Electrodeposited bumps are the indispensable microconnectors for high-density interconnection in the latest microelectronics applications.[1] For the higher frequency circuit, shorter interconnection length by bumps is required in order to reduce the reflection noise. Ball grid array (BGA) of solder bumps is necessary for high pin-count chips in order to reduce their packaging size. Bumps can also be used as a new testing method for bare chips of high pin-counts.[2] Another application is the interconnection between liquid crystal display (LCD) and driver chips, which are mostly interconnected with tape automated bonding (TAB). The bumps act as microconnectors of TAB technology and conduct digital signals from the chip to the LCD pixels.[3]

The bumps are electrodeposited onto the dot shaped cathode of 10 to 200 μm in diam. The cathode, or photolithography patterns, are patterned by photomask and photoresist. The control of electrodeposited bump shape, as well as the uniformity in their height, is important for obtaining proper interconnection reliability.[1]

The role of mass transport in etching of rectangular cavities formed by photoresist was extensively discussed by several authors. Alkire and Deligianni developed two-dimensional numerical fluid dynamics computations to study the electrolytic etching of copper.[4,5] The flow patterns were classified into two modes for the rectangular cavity of aspect ratios of 1.0 and 0.25, and their etch rate distribution numbers were compared. Alkire and Georgiadou reported the experimental results on chemical etching of copper.[6,7] They also developed numerical fluid dynamics computation to study the presence of sparingly soluble surface film and compared the average etch rate with experimental data for cavity aspect ratios of 1.0 and 0.20.[8] Shenoy and Datta studied the effect of mask wall angle on through-mask etching,[9] solving the primary current distribution numerically with boundary element method and discussing the etch factor with mask wall angle.

On the other hand, bumping is electrodeposition onto dots and rectangular cavities formed by photoresist. Dukovic developed a two-dimensional numerical computation of the tertiary current distribution. This distribution, however, does not include the convection. The moving boundary problem was discussed in regard to the shape evolution of copper electrodeposit and the effect of resist wall angle and leveling agent was reported.[10] The experimental studies on shape evolution of gold bumps were discussed by Kondo et al.[11] They studied the effects of dot diameter, electrolyte flow, and additive on bump shapes. The numerical fluid dynamics computation study on the initial stage of gold and copper bumps at Peclet numbers less than 100 were reported.[12,13] The numerical fluid dynamics computation study of copper bumps at higher Peclet numbers more than hundred was also reported.[14]

The present investigation discusses the shape evolution of copper bumps with photoresist angle. The role of outer diffusion, penetration flow, and vortex flows within the cavities is discussed in order to prevent side bumping, which is necessary for the high-density interconnection. Current distributions at diffusion controlled overpotentials were calculated by the numerical fluid dynamics computations.

Numerical Analysis

Two-dimensional cross sections of dot patterns are numerically analyzed by solving the equation of continuity, Navier-Stokes equations, and mass transfer equation

$$\frac{\partial u}{\partial x} + \frac{\partial v}{\partial y} = 0 \qquad [1]$$

$$\rho\left(u\frac{\partial u}{\partial x} + v\frac{\partial u}{\partial y}\right) = -\frac{\partial P}{\partial x} + \mu\left(\frac{\partial^2 u}{\partial x^2} + \frac{\partial^2 u}{\partial y^2}\right) \qquad [2]$$

* Electrochemical Society Active Member.

$$\rho\left(u\frac{\partial v}{\partial x} + v\frac{\partial v}{\partial y}\right) = -\frac{\partial P}{\partial x} + \mu\left(\frac{\partial^2 v}{\partial x^2} + \frac{\partial^2 v}{\partial y^2}\right) \quad [3]$$

$$u\frac{\partial c}{\partial x} + v\frac{\partial c}{\partial y} = D\left(\frac{\partial^2 c}{\partial x^2} + \frac{\partial^2 c}{\partial y^2}\right) \quad [4]$$

The computational area and the boundary conditions with resist angle θ are illustrated in Fig. 1. The details with resist angle of 90° are given in the Ref. 13 and 14. The numerical method proposed by Patankar[15] is adopted for discritization and pressure equation calculation. Smaller grid line spaces at the vicinity of both cathode and photoresist surface and also double precision variables calculation are adopted in order to reduce computational error. The Peclet number is defined as

$$\mathrm{Pe} = h\mathbf{u}_{y=2h}/D \quad [5]$$

The bump factor, a factor to represent the side bumping, is defined as

$$\mathrm{BF} = (i_{\mathrm{left}} + i_{\mathrm{right}})/(2i_{\mathrm{center}}) \quad [6]$$

Results and Discussion

Stream functions and isoconcentration contours with Pe numbers.—Figure 2 illustrates the normalized stream functions for the Pe numbers of 1.31, 41.6, and 7311 in (a), (b), and (c), respectively. Cathodes 100 μm in width are located at the cavity bottoms and 10 μm height photoresists are located on both sides of the cathode. The stream functions indicate the trajectory of fluid flow. The electrolyte flows from left to right as indicated by the arrows.

Vortices occur both at up and downstream corners.[12-14] The stream functions indicated at 6 are the penetration flows that start from the upstream side bulk solution to the cathode centers at cavity bottoms and to the downstream side bulk solution. The vortices at upstream side corners increase and grow toward the downstream side with the increase in the Pe numbers. The vortices at downstream side corners, on the other hand, decrease with the increase in the Pe numbers.

Figure 3 shows the isoconcentration contours of the Pe numbers of 1.31, 41.6, and 7311 in Fig. 3a, b, and c, respectively. The isoconcentration contours illustrate how the electrolyte is consumed on the cathodes at the cavity bottoms and how the concentration boundary layers develop. The isoconcentration contours converge and come close to the cathode with the increase in the Pe numbers.

Isoconcentration contours and stream functions with resist angle.—Figure 4 shows isoconcentration contours for the resist angle of −10 and 30° (Fig. 4a and b), respectively. The Pe numbers are 1.31 for both Fig. 4a and b. The mass-transport process is controlled mainly by diffusion for this small Pe number. Mass transport at the corners adds the diffusion from the outer surroundings, if compared at the center. This additional diffusion is shaded by the resist sidewall with negative resist angles of θ (Fig. 4a). On the other hand, this diffusion is enhanced with positive resist angles (Fig. 4b). Shading and enhancement of the outer diffusion is illustrated with closeness of adjacent contours. The adjacent contours are much closer at the cathode corner for the positive resist angle of Fig 4b than for that of Fig. 4a (arrows in Fig. 4). This closeness indicates larger current on the cathode corners.

Figure 5 shows the normalized stream functions for resist angles of −10 and 30° for Fig. 5a, b and c, d, respectively. The Pe numbers are 41.6 and 1407 for Fig. 5a, c and b, d, respectively. Vortices occur both at up and downstream side corners. The vortices increase for the cases of

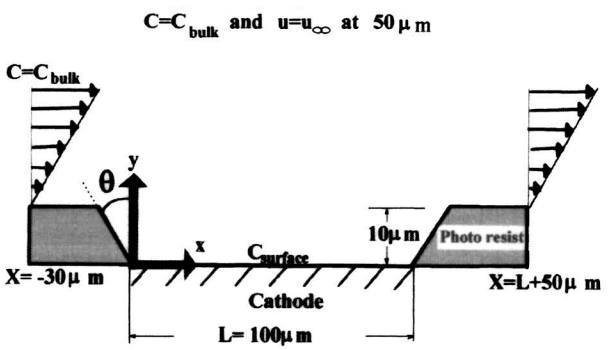

Fig. 1. Schematic illustration of two-dimensional cross section of photoresist and cathode. Resist angle of θ, *x* and *y* coordinates, and boundary conditions are shown.

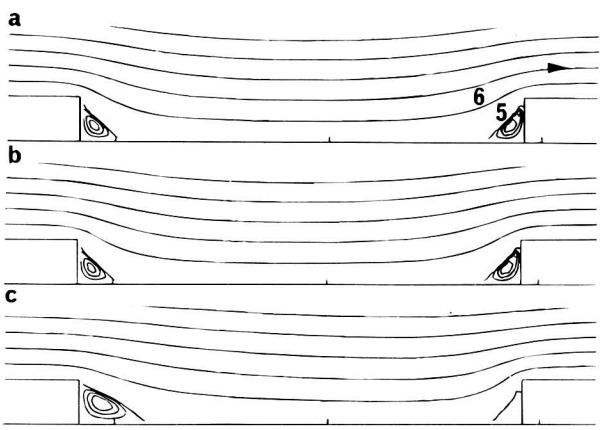

Fig. 2. Normalized stream functions for 100 μm cavity width; (a) Pe = 1.31, (b) Pe = 41.6, and (c) Pe = 7311.

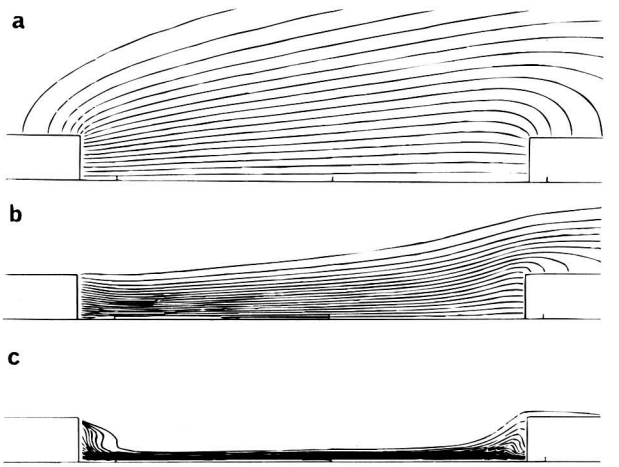

Fig. 3. Isoconcentration contours for 100 μm cavity width; (a) Pe = 1.31, (b) Pe = 41.6, and (c) Pe = 7311.

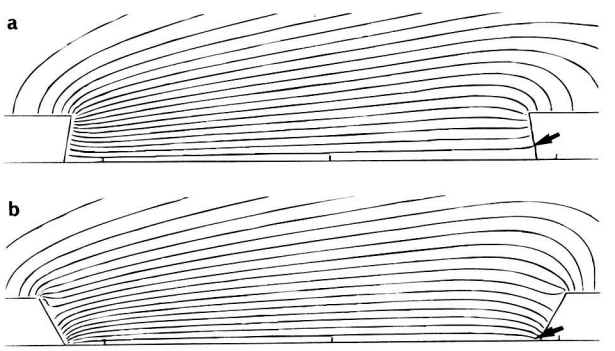

Fig. 4. Isoconcentration contours with different resist angles for Pe = 1.31; (a) θ = −10° and (b) θ = 30°.

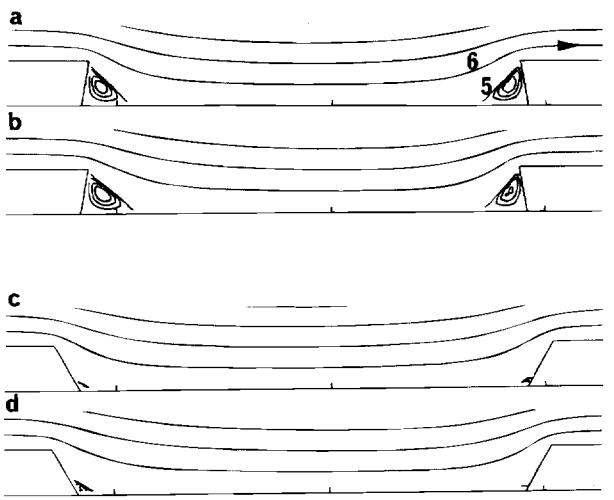

Fig. 5. Normalized stream functions with different resist angles for Pe = 41.6 and 1407; (a, b) θ = −10° and (c, d) θ = 30°.

the resist angle of −10°, but on the other hand, decreases for 30°. These vortices circulate within themselves and introduce local mass-transfer resistance of electrolyte to the cathode. The stream function 6 is the penetration flow.

The normalized stream functions (Fig. 2) and isoconcentration contours (Fig. 3) are obtained by changing Pe numbers. The isoconcentration contours are obtained for small Pe number of 1.31 by changing resist angles (Fig. 4). Furthermore, the normalized stream functions are obtained for Pe = 41.6 and 1407 by changing resist angles (Fig. 5). Based on these results, the current distributions at Pe = 1.31, 41.6, and 1407.2 are discussed in the following sections.

Current distributions at Pe = 1.31.—Figure 6 is the current distributions for the Pe number of 1.31. The mass-transport process is mainly controlled by diffusion for this small Pe number. For the resist angle of −10° of Fig. 6 (a), a decrease in current distribution is observed at upstream corner of x = 0 μm and gradually decrease toward downstream side. A small decrease is also observed at downstream corner of x = 100 μm. The diffusion from the outer surroundings is shaded by the resist sidewalls and causes this decrease. The penetration flow causes a gradual decrease toward downstream side.[12-14]

For the resist angle of 0° of Fig. 6 (b), the resist sidewalls do not shade the outer surroundings diffusions. The current distributions at both corners are flattened. For the resist angle of 30° of Fig. 6 (c), the surroundings diffusions are enhanced by the positive resist angle and sharp increases in current distribution exist at both corners.

Current distributions at Pe = 41.6.—Figure 7 is the current distributions for the Pe number of 41.6. The process is controlled both by diffusion and convection. For the resist angle of −10° of Fig. 7 (a), a large decrease at the upstream corner and a gradual decrease in current distribution toward the downstream side is observed. A small decrease in current distribution also exists at the downstream corner. The vortices occur at up and downstream corners (Fig. 5a, b). Not only these vortices, but also the shading of surrounding diffusion (Fig. 4a), causes these decreases.

For the resist angle of 0° of Fig. 7 (b), the resist sidewalls do not shade the surroundings diffusions. The current distribution decreases because of the vortices at the up and downstream corners. For the resist angle of 30° of Fig. 7 (c), the vortices reduce (Fig. 5c, d). The positive resist angle enhances diffusion from the surroundings (Fig. 4b) and current density shows sharp increases at both corners.

Current distributions at Pe = 1407.2.—Figure 8 is the current distributions for the Pe number of 1407.2. The process is mainly controlled by convection. For the resist angle of −10° of Fig. 8 (a), a large decrease at the upstream corner and the gradual decrease in current distribution toward the downstream side is observed. This large decrease is caused by vortices. The current distribution shows a small rise at downstream corner. This small rise is due to the vortex reduction at downstream corner (Fig. 2c). This vortex reduction is due to the collision between the penetration flows and the photoresist side walls at the downstream corner.[14]

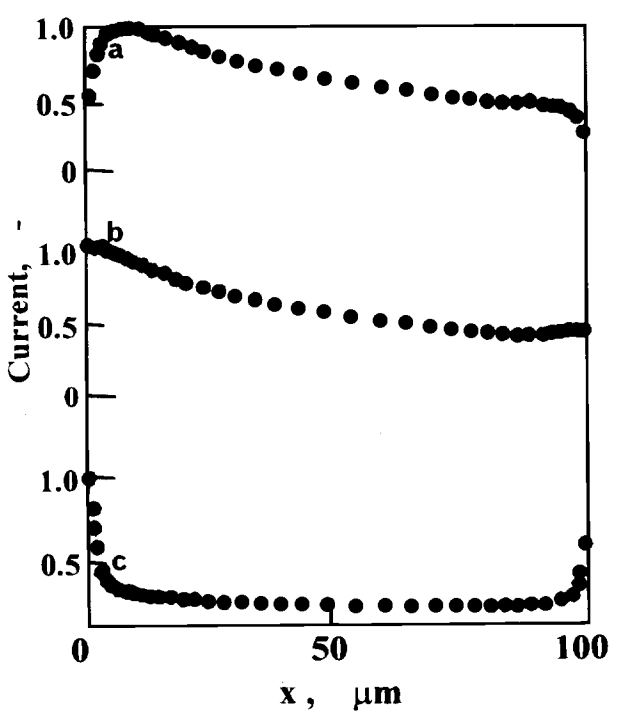

Fig. 6. Current distributions for 10 μm cavity width of Pe = 1.31 with different resist angles: (a) θ = −10°, (b) θ = 0°, and (c) θ = 30°.

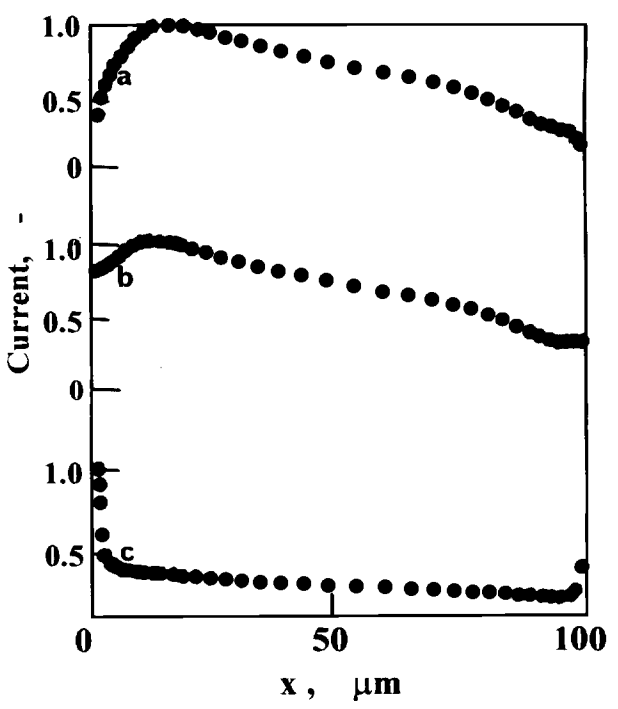

Fig. 7. Current distributions of Pe = 41.6 with different resist angles: (a) θ = −10°, (b) θ = 0°, and (c) θ = 30°.

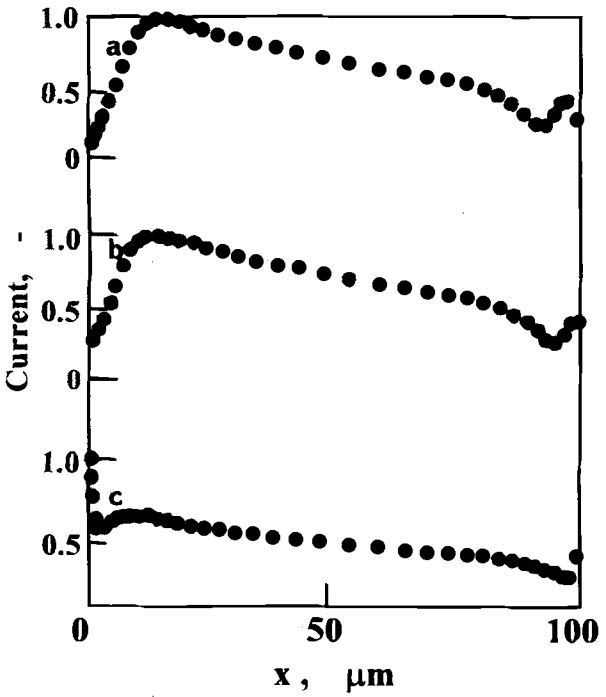

Fig. 8. Current distributions of Pe = 1407.2 with different resist angles: (a) θ = −10°, (b) θ = 0°, and (c) θ = 30°.

For the resist angle of 0° of Fig. 8 (b), the same current density behavior is observed as Fig. 8 (a). The vortices, however, decrease for the resist angle of 30° of Fig. 8 (c) (Fig. 5c, d). At the upstream corner, the current distribution shows sharp increase because of the diffusion from the surroundings (Fig. 4b). The current shows the minimum and a small rise toward downstream side because of the vortex formation. At the downstream corner, the vortex again causes a minimum and the surroundings diffusion causes a small rise.

Bump factor.—The amount of side bumping can be represented by the bump factors. Figure 9 summarizes a relation of bump factor (BF) and resist wall angle. The BF decreases as the decrease in resist wall angles. For small Pe number of 1.31, whose mass transport is controlled by the diffusion, the BF decreases monotonically as the decrease in resist wall angle.

For larger Pe numbers of 41.6 and 1407, the BF decreases because of the formation of vortices. The zero or negative resist angle enhances the vortices formation (Fig. 5a, b). These vortices are the local mass-transfer resistance to the cathode. The BF especially show small values for these zero or negative resist angles.

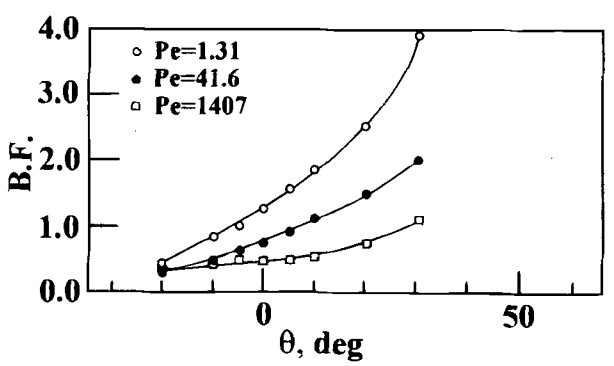

Fig. 9. Relation between BF and resist angle for Pe = 1.31, 41.6, and 1407.

Summary

The relation between resist wall angles and current distributions was discussed based on the numerical fluid dynamics computations. The role of outer diffusion, penetration flow, and vortex flows within the cavities was discussed in order to prevent side bumping.

1. Additional diffusion from the outer surroundings exists at the corners for the Pe number of 1.31. This outer diffusion is shaded by the negative resist sidewall angle of −10° and is enhanced with a positive angle of 30°. Vortices occur both at up and downstream side corners for the Pe numbers of 41.6 and 1407. The vortices increase for the angle of −10° and decrease for 30°. These vortices are the local mass-transfer resistance to the cathode.

We conclude that in order to prevent side bumping, the resist wall angles should be zero or negative. These zero or negative angles shade the outer diffusion and increase the vortices. These angles reduce the current at the cathode corner.

2. For a Pe number of 1.31, the process is mainly controlled by diffusion. A decrease in current distribution is observed at upstream corner for the negative angle of −10°. A decrease is also observed at downstream corner. The diffusion from the outer surroundings is shaded by this negative angle sidewall. The diffusion from the outer surroundings is shaded by this negative angle sidewall. For the positive angle of 30°, the surroundings diffusions are enhanced by this angle and sharp increases in current distribution exist at both corners.

3. For a Pe number of 41.6, the process is controlled by both diffusion and convection. A large decrease in current distribution at the upstream corner is observed, for the angle of −10°. A decrease in current distribution also exists at the downstream corner. Not only the vortices at up and downstream corners, but also the shading of the surrounding diffusion, causes these decreases. For the sidewall with an angle of 30°, the vortices reduce. This angle enhances diffusion from the surroundings and the current density shows a sharp increase at both corners.

4. For the Pe number of 1407.2, the process is mainly controlled by convection. A large decrease in current distribution at the upstream corner, caused by vortices, is observed for the angle of −10°. The current distribution shows a small rise at downstream corner. The vortices, however, decrease for the angle of 30°. At the upstream corner, the current distribution shows a sharp increase because of the diffusion from the surroundings. The current shows the minimum because of the vortex formation. At the downstream corner, the vortex causes a minimum and the surroundings diffusion causes a rise in the current distribution.

Acknowledgments

The authors thank Professor R. C. Alkire and his research group for the instructive discussions. Financial support from the Okayama Foundation for Science and Technology is gratefully acknowledged.

Manuscript submitted July 14, 1997; revised manuscript received November 12, 1997.

University of Okayama assisted in meeting the publication costs of this article.

LIST OF SYMBOLS

c	concentration, mol m^{-3}
D	diffusion coefficient, m^2/s^{-1}
h	resist height, m
i	current density, mA/cm^2
L	cathode length, m
Pe	$= hu_{y=2h}/D(-)$
u	velocity in the x-direction, m s^{-1}
v	velocity in the y-direction, m s^{-1}
x	coordinate in the streamwise direction, m
y	coordinate normal to the cathode surface, m
θ	resist angle (°)

REFERENCES

1. R. R. Tummala and E. J. Rymaszewski, *Microelectronics Packaging Handbook*, p. 361, Van Nostrand Reinhold, New York (1989).

2. Y. Yamamoto, M. Sugimoto, and K. Miyake, in *Proceedings of ISHM '93*, p. 370, Dallas, TX (1993).
3. K. Hatada, *Introduction to TAB Technology*, Kougiyou-chiyousakai, Tokyo (1989).
4. R. C. Alkire and H. Deligianni, *This Journal*, **135**, 1093 (1988).
5. R. C. Alkire, and H. Deligianni, and J-B. Ju, *ibid.*, **137**, 818 (1990).
6. M. Georgiadou and R. C. Alkire, *ibid.*, **140**, 1340 (1993).
7. M. Georgiadou and R. C. Alkire, *ibid.*, **140**, 1348 (1993).
8. M. Georgiadou and R. C. Alkire, *ibid.*, **141**, 679 (1994).
9. R. V. Shenoy and M. Datta, *ibid.*, **143**, 544 (1996).
10. J. O. Dukovic, *IBM J. Res. Develop.*, **37**, 125 (1993).
11. K. Kondo, T. Miyazaki, and Y. Tamura, *This Journal*, **141**, 1644 (1994).
12. K. Kondo and K. Fukui, *Kagaku Kogaku Ronbunshu*, **22**, (1996).
13. K. Kondo, K. Fukui, K. Uno, and K. Shinohara, *This Journal*, **143**, 466 (1997).
14. K. Kondo, K. Fukui, M. Yokoyama, and K. Shonohara, *ibid.*, **144**, 466 (1997).
15. S. V. Patankar, *Numerical Heat Transfer and Fluid Flow*, Hemisphere Publishing Corp., New York (1980).

Self-Discharge of Sealed Nickel–Metal Hydride Batteries

Mechanisms and Improvements

Patrick Leblanc,[a] Philippe Blanchard,[a] and Stéphane Senyarich[b]

[a]*SAFT, Research Department, 91460 Marcoussis, France*
[b]*SAFT, Portable Batteries Technical Division, 16440 Roullet St-Estéphe, France*

ABSTRACT

Mechanisms likely to accelerate self-discharge of a nickel–metal hydride (Ni–MH) battery have been investigated. A higher self-discharge rate of sealed Ni–MH batteries compared to Ni–Cd is explained by shuttle reactions between nitrite ions and ammonia. Even if a polyolefin separator stable in the electrolyte is used, the positive electrode is an important source of nitrogen impurities. It was found that some grafted polyolefin separators have a special ability to trap ammonia. Using this specially designed separator and provided that the entire quantity of ammonia can be trapped, the self-discharge rate of Ni–MH batteries can be reduced to the self-decomposition of the charged active material in the positive electrode.

Introduction

Nickel–metal hydride (Ni–MH) batteries using hydrogen storage alloys yield a higher energy density than Ni–Cd batteries and favorably replace Ni–Cd cells in portable appliances. However, higher self-discharge rates are often reported in Ni–MH batteries. Several papers have been published on the subject, but conclusions are contradictory. It has been reported that the self-discharge of sealed Ni–MH batteries is accelerated by ammonia and amine ions which participate in redox shuttle reactions.[1,2] Based on this mechanism, the use of stable polyolefin separators which do not produce ammonia during degradation have been recommended.[3,4] The use of battery components depleted in nitrogen impurities,[5] as well as cell-design modifications,[6] have also been proposed in order to improve self-discharge of MH batteries. On the other hand, other workers have concluded that the chemical reaction between H_2 and the charged positive active mass is the main reason for the high self-discharge rate.[7-9]

In this work, mechanisms likely to accelerate self-discharge are clearly identified: (*i*) self-decomposition (thermodynamic instability) of the positive electrode leading to a release of oxygen which ultimately reacts with the negative electrode, (*ii*) reduction of the positive electrode by hydrogen gas coming from the MH electrode, and (*iii*) redox shuttles.

The contribution of each of these mechanisms to self-discharge has been evaluated and the most dominant has been identified. In light of these results, practical solutions for reducing the self-discharge rate to a level comparable to Ni–Cd cells are proposed.

Experimental

Ni–MH sealed cylindrical cells with a typical capacity of 1.2 Ah (AA size) were used for battery self-discharge measurements. These batteries were obtained by spirally winding a nickel hydroxide positive electrode and a hydrogen-storage alloy negative electrode along with a polyamide or a polyolefin separator. The electrolyte used was a ternary 8.7 M KOH, 0.5 M NaOH, 0.5 M LiOH aqueous solution with 9.9 N total normality.

The composition of the hydride-forming alloy used in the negative electrode was $MmNi_{3.55}Mn_{0.4}Al_{0.3}Co_{0.75}$ (Mm: misch metal). Spherical nickel hydroxide containing 0.75% coprecipitated Co and 3% coprecipitated Zn was used as a standard positive active material.

For self-decomposition measurements of the positive electrodes, positive foam electrodes containing spherical nickel hydroxide powders were initially fully charged at the 0.1 C rate for 16 h in half-cells using Cd counter electrodes and a polyolefin separator. The cell was disassembled and the positive electrode was partially immersed in the electrolyte for 7 days at 40 °C in a container continuously purged by air or hydrogen or argon. In order to avoid electrolyte carbonation or evaporation, the gas was allowed to bubble in a separate flask containing the same electrolyte at 40 °C before introduction to the container.

Nitrate and nitrite ions concentrations were determined by ionic chromatography using a Dionex 100 apparatus with a AS4A-SC column. The ammonia content was measured by Kjeldhal's technique using a Büchi distillation unit.

Self-discharge rates of positive plates or AA cells were evaluated after a week's storage at 40 °C. The remaining discharge capacity after storage was measured at the 0.2-C rate and compared to the discharge capacity before storage.

Results and Discussion

Self-decomposition of the positive electrode.—It is known that the charged nickel hydroxide electrode is not thermodynamically stable in the electrolyte. A decrease in the state of oxidation of the positive material is observed, and O_2 gas evolution takes place according to eq 1

$$NiOOH + \frac{1}{2}H_2O \rightarrow Ni(OH)_2 + \frac{1}{4}O_2 \qquad [1]$$

Conway and Bourgault showed that the oxygen evolution reaction was the rate-determining step in the self-discharge of nickel oxyhydroxide.[10]